Fluid flow in a tube with an elastic membrane insertion

By GIANNI PEDRIZZETTI

Dipartimento Ingegneria Civile, Università di Firenze, Via Santa Marta 3, 50139 Firenze, Italy

The unsteady flow of a viscous incompressible fluid in a circular tube with an elastic insertion is studied numerically. The deformation of the elastic membrane is obtained by the theory of finite elasticity whose equations are solved simultaneously with the fluid equations in the axisymmetric approximation. The elastic wall expands outwards due to the positive transmural pressure and represents an idealized model for the response of pathologies in large arteries.

It is found that if either the fluid discharge or the reference pressure are imposed downstream of the insertion, the fluid–wall interaction develops travelling waves along the membrane whose period depends on membrane elasticity; these are unstable in a perfectly elastic membrane and are stabilized by viscoelasticity. In the reversed system, when the fluid discharge is imposed on the opposite side, the stable propagation phenomenon remains the same because of symmetry arguments. Such arguments do not apply to the originally unstable behaviour. In this case, even when the membrane is perfectly elastic, propagation is damped and two natural fluctuations appear in the form of stationary waves. In all cases the resonance of the fluid–wall interaction has been analysed. Comparisons with previously observed phenomena and with results of analogous studies are discussed.

1. Introduction

The hydraulics of steady and unsteady motion in elastic conduits is of relevance in many fields. Its primary applications are to cardiovascular systems to understand the evolution of pathology due to vessel deformation or the hydraulic behaviour after the insertion of an elastic prosthesis. The presence of a compliant wall also influences the stability of the boundary layer, delaying the development of laminar–turbulent transition (Davies & Carpenter 1997 and references therein). In general an elastic membrane connecting two rigid ducts represents a mechanical filter and understanding it may be useful in several applications.

The calculation of the simultaneous fluid–structure evolution has many difficulties and, despite the theoretical and practical relevance, very few results have been produced on fluid motion in elastic tubes. The development of a computational technique able to deal with such a system also motivated the present work.

The linear theory (Lighthill 1978) provides some basic information about one-dimensional waves in elastic tubes. The resonating phenomenon in a finite length membrane has been predicted analytically using a perturbative approach (Secomb 1978), and the outcome shows qualitative agreement with some features observed in coronary flow. The existence and the stability of steady configurations in a collapsible tube have been analysed using one-dimensional models. In Reyn (1987) the membrane

was carefully modelled but the fluid was reduced to a Bernoulli balance; an attempt to incorporate dissipative phenomena in one-dimensional models has been proposed in Cancelli & Pedley (1985) and Jensen & Pedley (1989). One-dimensional models can partially take into account the dynamics of the separated vorticity and its interaction with the wall only by introducing ad hoc assumptions; thus additional information either experimental or numerical is necessary for the improvement of simple models and for the verification of the results.

The steady flow in a two-dimensional channel with a non-rigid wall on one side has been carefully analysed in Luo & Pedley (1995) by a coupled steady solution of the Navier–Stokes equations and a membrane law using the finite element method. The wall is there assumed to have a constant tension and a limiting small value, corresponding to a very compliant elastic membrane, for the existence of a steady solution has been determined. The study has been extended to unsteady flow (Luo & Pedley 1996) in which case the constant tension assumption corresponds to a free-surface boundary. That work is devoted to the collapse phenomenon in veins and to the development of self-excited oscillation in the proximity of collapsing parameters. It differs from the one presented here which treats elasticity phenomena in tubes under pressure (i.e. arteries); however the computational technique has some analogies with the present one, which will be described.

The stability of fluid–structure interaction in the presence of a compliant wall has been studied in a series of articles. Carpenter & Morris (1990) have shown by a stability analysis of Tollmien–Schlichting waves that the presence of a compliant wall can substantially increase the value of the transitional Reynolds number. A two-dimensional simulation of such a problem has been performed in Davies & Carpenter (1997) where the coupled fluid–wall problem has been solved using a linearized form of the Navier–Stokes equations. If the wall is sufficiently compliant the instability of Tollmien–Schlichting waves can, in principle, be arbitrarily delayed; however, other types of instability can be possible and can trigger laminar–turbulent transition (Lucey & Carpenter 1992). These works show two new types of boundary layer instability over a compliant wall: travelling-wave flutter which has a phase speed close to the free-stream velocity and a quasi-stationary wave usually called divergence. An extensive stability analysis of the laminar flow in flexible tubes (Kumaran 1996 and references therein) has shown that the classical inflection point results on the stability of steady velocity profiles are modified by the presence of fluid–wall interaction. Several results, pointing out the role of viscosity, are given for the growth of axisymmetric and three-dimensional disturbances. These studies deal with the local-in-space stability of steady velocity profiles (expressed in series of a perturbation parameter) and cannot be expressed directly in terms of global quantities; a comparison with the results of the numerical solution, even if possible after manipulation of the data, is outside the scope of the present work.

The present work is focused on the steady and unsteady flow in a tube with a finite length membrane inserted in the otherwise rigid duct. The analysis is performed through the simultaneous numerical solution, in the axisymmetric approximation, of the incompressible Navier–Stokes and membrane equations. The system is numerically approximated by finite differences and the membrane movement is evaluated within the theory of finite elasticity (Green & Adkins 1960) with no assumption about its geometry or wall movement.

The purpose of this work is the theoretical determination of some of the many phenomena that occur in the interaction between the fluid flow and the elastic movable wall. The motivation derives from the evolution of pathologies in large

arteries and the fluid mechanical disturbances induced by local vessel reconstruction; nevertheless this study is essentially theoretical, and is devoted to the identification of some physical phenomena involved, and their dependence on the parameters.

The theory of a membrane under finite deformation is based on a static analysis and little is known experimentally about the influence of the unavoidable viscous resistance to dynamic strain. The influence of viscoelastic membrane behaviour on the time evolution and stability of the system is analysed here. Then the formation and propagation of waves over the wall and the unsteady resonance phenomenon is investigated.

The presence of an elastic insertion requires the definition of the value of pressure at two positions along the tube; in numerical calculations this is usually transformed, for simplicity, to the definition of pressure in one reference section and flow rate in a second one. In a rigid duct the actual pressure value has no influence and flow rate is constant along the tube; in the present elastic case the relative, upstream or downstream, positioning of these conditions has a relevant and not intuitive role which is analysed here and discussed.

The mathematical formulation for the fluid problem and membrane law is presented in §2 with a preliminary discussion of the variation of the physical dimensionless parameters. The numerical method for the simultaneous computation of the fluid–membrane system is introduced in §3. The results from the numerical simulations are reported in §4. Discussions are developed through the paper; conclusions and a summary of the most relevant issues are given in §5.

2. Mathematical formulation

2.1. *General specifications*

Consider the flow of an incompressible viscous fluid, with density ρ and kinematic viscosity v, moving with a time-averaged mean velocity U_0 inside a tube with rectilinear axis and circular cross-section of radius R_0. Before any further specification let us formulate the problem in dimensionless terms by assuming a unit of length R_0, a unit of time R_0/U_0, and a unit of mass ρR_0^3. In what follows all quantities are implicitly assumed in dimensionless units unless otherwise stated.

The tube is assumed to extend infinitely far both upstream and downstream; the tube wall is assumed to be perfectly rigid everywhere apart from a portion of length L where the rigid wall is substituted with a membrane which deforms because of transmural pressure and because of shear stress.

The x-axis is chosen coincident with the tube axis and with the origin at the centre of the membrane which extends from $x = -L/2$ to $x = +L/2$. A reference transmural pressure p_{ref} is assumed one diameter downstream of the insertion at a position $x_{ref} = L/2 + 2$, and a value of the velocity averaged over the cross-section

$$U(t) = 1 + \varepsilon \sin(2\pi S_t t), \tag{1}$$

is imposed in the downstream rigid portion of the tube. In §4.3 the law (1) is imposed upstream and also the effect of an upstream reference pressure is discussed. The Strouhal number S_t in (1) represents the dimensionless frequency of forced flow oscillation, of amplitude ε, superimposed on the steady flow.

2.2. *Fluid equations*

Assume the duct axis as the x-axis of a cylindrical system of coordinates $\{x, r, \theta\}$; the approximation of axial symmetry makes the flow independent of the θ coordinate.

The governing equations for the fluid are the axisymmetric form of the Navier–Stokes equations which are written in the vorticity–streamfunction formulation (Batchelor 1967; Panton 1996)

$$\frac{\partial \omega}{\partial t} + \frac{1}{r}\frac{\partial \psi}{\partial r}\frac{\partial \omega}{\partial x} - \frac{1}{r}\frac{\partial \psi}{\partial x}\frac{\partial \omega}{\partial r} + \frac{\omega}{r^2}\frac{\partial \psi}{\partial x} = \frac{1}{R_e}\left(\frac{\partial^2 \omega}{\partial x^2} + \frac{\partial^2 \omega}{\partial r^2} + \frac{1}{r}\frac{\partial \omega}{\partial r} - \frac{\omega}{r^2}\right), \quad (2)$$

where $\omega(x, r, t)$ is the azimuthal vorticity and $\psi(x, r, t)$ is the Stokes streamfunction; the Reynolds number R_e is here defined as

$$R_e = \frac{R_0 U_0}{v}, \quad (3)$$

vorticity and streamfunction are related by the Poisson equation

$$-\omega\, r = \frac{\partial^2 \psi}{\partial x^2} + \frac{\partial^2 \psi}{\partial r^2} - \frac{1}{r}\frac{\partial \psi}{\partial r}. \quad (4)$$

Equations (2) and (4) must be completed with the boundary conditions. Infinitely far upstream and downstream, where the tube is cylindrical, the velocity profile is assumed as constant along x. On the axis of the duct, $r = 0$, the boundary conditions are given by symmetry considerations

$$\omega(t, x, r = 0) = 0, \quad \psi(t, x, r = 0) = 0. \quad (5)$$

At the wall the fluid velocity vector must be equal to the membrane velocity. The tube wall is specified by a function $R(t, x)$ representing the tube radius at time t at a position x along the tube axis; this function is identically unity along the rigid walls and is a two-dimensional function for the membrane. The boundary conditions at the wall are better expressed by choosing a system of coordinates where the moving wall coincides with a constant coordinate curve.

We apply a shearing coordinate transformation (Eiseman 1985) replacing the r-coordinate with a new z-coordinate defined by

$$z = \frac{r}{R(t, x)}, \quad (6)$$

in the new system of coordinates $\{t, x, z\}$ the z-direction is non-orthogonal both to the time direction and spacial x-direction. Equations (2) and (4) can be rewritten in this new system of coordinates by using the composite derivatives rule.

The new coordinates permit an easier introduction of the boundary conditions at the wall $z = 1$. Let us call the instantaneous axial and radial membrane velocity $U_x(t, x)$ and $U_r(t, x)$; the no-slip condition gives

$$\frac{\partial \psi}{\partial x} = R\left(R' U_x - U_r\right), \quad \frac{\partial \psi}{\partial z} = R^2 U_x, \quad (7)$$

where the prime is used to denote the x-derivative. The first of conditions (7) is sufficient for the solution of the Poisson equation once the value of the streamfunction is given at one point. This is done by imposing the section-averaged velocity (1) downstream of the membrane:

$$\psi(t, x > L/2, z = 1) = \frac{U(t)}{2}. \quad (8)$$

The value of the wall vorticity is obtained by writing the Poisson equation at the wall

$$\omega(t, x, z = 1) = -\frac{1}{R}\left\{ \frac{\partial}{\partial x}\left(\frac{\partial \psi}{\partial x}\right) - 2\frac{R'}{R}\frac{\partial}{\partial x}\left(\frac{\partial \psi}{\partial z}\right) + \frac{2R'^2 - RR'' - 1}{R^2}\frac{\partial \psi}{\partial z} \right.$$
$$\left. + \left[\left(\frac{\partial z}{\partial x}\right)^2 + \left(\frac{\partial z}{\partial r}\right)^2\right]\frac{\partial^2 \psi}{\partial z^2} \right\}. \tag{9}$$

The first three terms in equation (9) are given directly by conditions (7) and their x-derivatives; the last term must be evaluated from the streamfunction field as is the standard procedure during the numerical time marching (e.g. Fletcher 1988).

The mathematics of the fluid problem itself is thus completely described once the membrane velocities are known. Furthermore, the fluid acts on the movable membrane through the values of the normal stress, $\tau_n(t, x)$, and the tangential stress, $\tau_{tg}(t, x)$, at the wall. From the definition of the stress tensor in a Newtonian fluid (Panton 1996) we get, for a movable wall,

$$\tau_n = p + \frac{2}{R_e}\left(\frac{U'_x + R'U'_r}{1 + R'^2} + \frac{U_r}{R}\right), \tag{10}$$

$$\tau_{tg} = \frac{1}{R_e}\left(\omega - 2\frac{U'_r - R'U'_x}{1 + R'^2}\right). \tag{11}$$

The wall pressure, $p(t, x)$, in (10) is evaluated by integration of

$$\frac{\partial p}{\partial x} = -\dot{U}_x - R'\dot{U}_r - U_x\left(U'_x + R'U'_r\right) + \frac{1}{R_e}\left(R'\frac{\partial \omega}{\partial x} - \frac{1 + R'^2}{R}\frac{\partial \omega}{\partial z} - \frac{\omega}{R}\right), \tag{12}$$

starting from the reference value p_{ref}. Equation (12) is obtained by a combination of the Navier–Stokes equations written at the wall in primitive variables, and the dot is used to denote time derivatives.

2.3. *Membrane equations*

A membrane is a mathematical model for a solid shell of extremely small thickness such that it can be assumed as having no bending stiffness. A membrane supports only stresses parallel to its surface which are also assumed to be constant along the thickness. In the present work the membrane is assumed inertialess. Such an assumption means that the total membrane mass is negligible with respect to the mass of the fluid which accelerates during the motion. It has been verified in the limit of extremely small membrane thickness (Luo & Pedley 1996). In such a scheme the membrane deforms to be constantly in equilibrium with the external loads.

In order to apply the general equations for a membrane with finite deformation in the axisymmetric case (Green & Adkins 1960), let us introduce a parametric coordinate s along the membrane such that in different deformed configurations the points with the same value of s always correspond to the same material particle. The axial and radial coordinates of the material particle are denoted with $x_p(t, s)$ and $r_p(t, s)$, where the subscript p is used to indicate that coordinates are associated with particles. Because of the axial symmetry of the membrane and of the external loads, the meridional and circumferential directions are eigendirections of the deformation

gradient tensor. The principal deformation ratios are thus given by

$$
\left.
\begin{aligned}
\lambda_1(t,s) &= \left[\left(\frac{\partial x_p}{\partial s}\right)^2 + \left(\frac{\partial r_p}{\partial s}\right)^2\right]^{1/2}, \\
\lambda_2(t,s) &= \frac{r_p(t,s)}{R_u},
\end{aligned}
\right\}
\tag{13}
$$

where the subscripts 1 and 2 indicate meridional and circumferential directions, respectively. The parameter R_u represents the value of the radius in the undeformed membrane; in what follows it is assumed that $R_u = 1$.

An elastic material is characterized by a constitutive law expressed in the form of a strain–energy relation. In general the elastic energy of a mathematically admissible material should be expressed as a function of the invariants of the deformation tensor (Green & Adkins 1960); in the simpler case of an incompressible isotropic membrane the elastic energy can be expressed in terms of the eigenvalues as $W(\lambda_1, \lambda_2)$ (Pipkin 1968). From the strain–energy relation we can evaluate the strain–stress relation by

$$
T_1 = \frac{1}{\lambda_2}\frac{\partial W}{\partial \lambda_1}, \quad T_2 = \frac{1}{\lambda_1}\frac{\partial W}{\partial \lambda_2},
\tag{14}
$$

where T_1 and T_2 are the membrane stresses (stresses integrated over the local deformed thickness) along the principal directions. Equations (14) are valid for an isotropic incompressible material; otherwise the principal directions of strain and stress may not coincide and more general relations should be employed (Humphrey, Strumpf & Yin 1992). Equations (14) must be introduced in the equilibrium equations (Green & Adkins 1960) to determine the membrane deformation. Before doing this a preliminary rearrangement is introduced here.

The formulation described above is written in terms of Lagrangian coordinates, i.e. material particles, whereas the wall geometry in the fluid problem is expressed in terms of Eulerian quantities with the longitudinal coordinate x as the independent variable. We perform an Eulerian transformation of the membrane formulation introducing the functions $R(t,x)$ and $S(t,x)$ which are related to the Lagrangian coordinates in the following manner:

$$
R\left[t, x_p(t,s)\right] = r_p(t,s), \quad S\left[t, x_p(t,s)\right] = s.
\tag{15}
$$

Note that the function $R(t,x)$ is now the same as introduced in the fluid problem above. Following (15), the principal deformation ratios (13) can be expressed in terms of Eulerian variables as

$$
\lambda_1(t,x) = \left(\frac{1 + R'^2}{S'^2}\right)^{1/2}, \quad \lambda_2(t,x) = \frac{R(t,x)}{R_u}.
\tag{16}
$$

The membrane velocities introduced in §2.2 are the instantaneous material velocity of the membrane, i.e. $U_x = \partial x_p/\partial t$ and $U_r = \partial r_p/\partial t$; these can be expressed in terms of Eulerian variables by time differentiation of relations (15) which results in

$$
\dot{R} = U_r - R'U_x, \quad \dot{S} + S'U_x = 0.
\tag{17}
$$

The equilibrium equations can be readily written in terms of Eulerian variables. The equilibra in the tangential direction and in the normal direction are given by

$$
\left.\begin{array}{r}
R'\left(T_1 - T_2\right) + R T_1' = \tau_{tg} R R', \\[2ex]
\dfrac{-R''}{\left(1 + R'^2\right)^{3/2}} T_1 + \dfrac{1}{R\left(1 + R'^2\right)^{1/2}} T_2 = \tau_n,
\end{array}\right\}
\tag{18}
$$

respectively. The terms which multiply the membrane stresses in the normal equilibrium are the corresponding curvatures of the membrane. The principle of minimum potential energy can be used as an alternative to the equilibrium equations (Tielking & Feng 1974, Fried 1982); however it can be easily expressed only for the case of uniform external loads and is not used here.

In order to solve the equilibrium membrane equations (18) an explicit expression for the constitutive strain–energy relation must be given. In the present work we employ

$$
W(\lambda_1, \lambda_2) = K \left\{ \frac{\lambda_1 \lambda_2}{2} (\lambda_1 + \lambda_2 - 3) + \frac{1}{2} \right\},
\tag{19}
$$

which corresponds to an incompressible linear elastic membrane (Hooke's law), K being the coefficient of elasticity which is equal to the dimensionless combination $Eh/\rho R_0 U_0^2$ where E is the Young modulus and h is the undeformed membrane thickness. Formula (19) does not imply that the analysis is restricted to small deformation but that the membrane is made of a linearly elastic material. It represents the simplest choice to identify a reference elastic behaviour to be used for comparison with possible future results employing nonlinear materials. In particular the simple Mooney–Rivlin relation is often applied to rubber-like materials where stiffness decreases with growing strain, while other relations appear to give a better representation, in static tests, for the hyperelasticity of biomembranes (Skalak *et al.* 1973; Hsu *et al.* 1994; Kyriacou & Humprey 1996).

The constitutive theory of finite elasticity, summarized in equations (14) and (19), is based on a static description of the solid material. In a moving membrane, even neglecting inertia, we should take into account the unavoidable presence of a viscous resistance to extremely rapid deformations of the material. In analogy with the elastic stress–strain relation we employ the following relation between strain and rate of strain with stress:

$$
\left.\begin{array}{l}
T_1(\lambda_1, \lambda_2, \dot\lambda_1, \dot\lambda_2) = K\left(\lambda_1 + \dfrac{\lambda_2}{2} - \dfrac{3}{2}\right) + C\left(\dot\lambda_1 + \dfrac{\dot\lambda_2}{2}\right), \\[2ex]
T_2(\lambda_1, \lambda_2, \dot\lambda_1, \dot\lambda_2) = K\left(\lambda_2 + \dfrac{\lambda_1}{2} - \dfrac{3}{2}\right) + C\left(\dot\lambda_2 + \dfrac{\dot\lambda_1}{2}\right),
\end{array}\right\}
\tag{20}
$$

where C is the viscosity coefficient. Note that the ratio C/K represents a time scale for the response of the membrane such that more rapid oscillations are damped by viscous resistance. In principle the fluid also gives a viscous resistance to the deformation of the membrane; however, we cannot say a priori if membrane viscosity is negligible with respect to the fluid one. In the simulations presented below the influence of the membrane viscosity is analysed in detail.

Appropriate boundary conditions must be introduced to evaluate the instantaneous deformation of the viscoelastic membrane by solving the equilibrium equations (18) with stresses given by the constitutive relations (20). At the two ends the membrane

must connect with the rigid tube:

$$R\left(-\tfrac{1}{2}L\right) = 1, \quad S\left(-\tfrac{1}{2}L\right) = 0, \left.\begin{array}{c}\\[1.5em]\end{array}\right\}$$
$$R\left(+\tfrac{1}{2}L\right) = 1, \quad S\left(+\tfrac{1}{2}L\right) = L_u. \tag{21}$$

The fourth of conditions (21) implies that a membrane of undeformed length L_u is used to cover the length L; however, in what follows it is assumed that $L_u = L$.

Conditions (21) ensure the continuity of the wall geometry at the rigid–elastic connections; nevertheless the derivative R' is not continuous and the wall presents a corner at such connections. From a physical point of view this can be achieved only by a very special kind of link like a toroidal hinge; experimentally the membrane is usually fastened to the rigid wall and presents a continuous, even if rapidly changing, first derivative. This contradiction occurs because the radius of curvature approaches zero at corners and the hypothesis of a membrane, i.e. thickness much smaller than longitudinal scales, is not valid at the rigid–elastic junctions. While conditions (21) are ensured by the action of forces at the rigid–elastic junctions, the continuity of the first derivative implies that a moment is also acting at the edge. Such an action cannot be achieved by a mathematical membrane which has zero bending stiffness while a real thin elastic solid is able to produce a moment as its radius of curvature becomes comparable with its thickness. Mathematically, the presence of a corner does not represent a problem for the membrane equations because the right (in the upstream edge) or left (downstream) values of R' are well defined. Rather, this represents a problem for the fluid equations because the jump in R' provokes a kink in the fluid variables.

To overcome this inconsistency in the coupled system the membrane formulation should be replaced, in principle, with one for a thin shell with bending stiffness. However, in the limit of vanishing thickness, the membrane approximation is valid everywhere with the exception of the material points adjacent to the rigid–elastic junctions where the approximation does not allow slope continuity. The simplicity of the membrane formulation is thus retained here for the inner points. The result of applying a shell model next to the edges would be that, dynamically, a non-zero moment reaction appears at the edge and, geometrically, wall slope is continuous. The presence of a moment at the edge has no influence on the tangential equilibrium while the normal equilibrium equation adjacent to the membrane end differs from the membrane one. Thus the normal equilibrium equation is substituted there with the condition of continuity of the slope so that the geometrical result of considering a thin shell is imposed explicitly.

The present model is a tentative one to represent a membrane model at the inner points matched to the result of a shell model adjacent to the junction. As stated before, its main purpose is to avoid a singular point for the fluid equations at the junctions. However, the discretization procedure itself can act as a low-pass filter which is able to smooth out the corners. In fact it has been verified, and we wish to stress this, that no substantial differences have been observed in the numerical results on either imposing the slope continuity or not apart from a sharper peak of vorticity at the edges in the latter case.

2.4. *Preliminary discussion on parameter values*

The physical system described above depends on a large number of dimensionless parameters; thus a preliminary analysis is necessary to identify and possibly to reduce their range of variation. We keep in mind that the present research, though of a

theoretical nature, has been primarily stimulated by phenomena of fluid–structure interaction in large human arteries and thus parameter variation will be confined to values of relevance for such conditions.

The fluid steady state is characterized by the Reynolds number only, having in mind the flow in the human carotid where the diameter is typically around 0.5 cm, and velocity about 0.5 m s^{-1}; the Reynolds number is here kept fixed to the value $R_e = 300$. The membrane elasticity parameter K ranges, in dimensionless units, from values larger than 10 up to some hundreds (Pedley 1980; Kyriacou & Humphrey 1996). In a human artery transmural pressure is usually positive, in dimensionless units, and using the aforementioned dimensional value for velocity, it ranges from a few units to values just under about 20 (Pedley 1980); this gives a physical indication for the reference pressure p_{ref}. The local radial deformation is approximately given by p/K. Thus the value of p_{ref} must be smaller than K to avoid unacceptable membrane deformations but it cannot be orders of magnitude smaller otherwise the tube remains undeformed; moreover p_{ref} must be larger than but comparable with pressure variations, in space and time, otherwise it remains the only parameter responsible for deformation and the fluid problem results uncoupled from the wall ones.

An indication for realistic values of the viscous parameter C can be obtained from a relation with elasticity and natural frequency observed in viscoelastic materials. This results in a range of values $[0.1, 0.5]$ times K/St. Actually such a range corresponds to significant viscoelastic phenomena; much smaller values give essentially no damping and much larger ones result in purely viscous material. The actual values will be taken about such a typical range and varied with respect to the stability of the system. In several applications the membrane length L can be though to be a multiple of the tube size; in what follows the value $L = 2$ is assumed. The undeformed membrane length $L_u = L$ is assumed, the undeformed membrane radius $R_u = 1$.

These figures produce a local enlargement of the elastic section, due to the positive transmural pressure, and the membrane is everywhere in traction. The membrane formulation is physically not acceptable if the wall becomes substantially compressed; the zero-bending stiffness makes a membrane unstable under compression, squeezing in a non-circular shape. A simplified one-dimensional pressure–area law for a compressed membrane is reported in Pedley (1980) on the basis of experimental observation.

The unsteady pulsatile flow in an artery has a Strouhal number of about 5×10^{-3}. Perturbations to the steady flow with Strouhal number around this value are extremely slow with respect to convective phenomena and thus such a type of unsteadiness can be accounted for in a quasi-steady analysis and does not require the solution of the coupled problem. The Strouhal number in equation (1) will be chosen comparable with the frequency of natural membrane oscillations in order to observe fluid–structure resonance phenomena; small values of the amplitude ε will be chosen to identify stable and unstable dynamics.

3. Numerical technique

3.1. *Fluid problem*

The computational domain in the $\{x, z\}$-plane is represented by the infinite strip $(-\infty, +\infty) \times [0, 1]$. A higher resolution is required close to the wall to resolve well the phenomenon of vorticity generation and separation; for this reason we introduce a

stretching of the z-axis with a new coordinate ζ defined by

$$z = \frac{\tanh(a\,\zeta)}{\tanh(a)}, \tag{22}$$

where a is a stretching parameter. The x-domain must extend very far from the expansion in both directions where the outlet and inlet boundary conditions will be specified. Nevertheless the flow is expected to become uniform far from the membrane, while a higher resolution is necessary for the moving wall and in particular at the elastic–rigid junctions. A stretching of the x-axis is introduced by using the new coordinate η defined by

$$x = b_1 \tanh^{-1} \left\{ \eta - b_2 \eta \left(\eta^2 - 1 \right) e^{-\eta^2 / b_3^2} \right\}, \tag{23}$$

where b_i, $i = 1, 2, 3$, are stretching parameters. The composite stretching function (23) allows a better resolution over the whole membrane length and also locates two regions of maximum resolution symmetrically about $x = 0$. In the new system of coordinates $\{\eta, \zeta\}$ a uniformly spaced rectangular grid is superimposed onto the $(-1, 1) \times [0, 1]$ domain.

The numerical formulation for the fluid problem strictly follows the one described in detail in Pedrizzetti (1996). Fluid equations are made discrete using centred second-order finite differences, the nonlinear Jacobian term in the equation of motion is made discrete using the dealiased Arakawa (1966) scheme, time is advanced using the low-storage third-order Runge–Kutta method. At the wall, $\zeta = 1$, vorticity boundary conditions are given by (9) where the second-order transversal derivative is evaluated by standard Taylor approximation (Fletcher 1988). Both first- and second-order truncations have been checked, giving no essential differences because the grid refinement near the wall ensures small truncation error; however during rapid transients the first-order approximation presented a better and more stable convergence, as discussed in Fletcher (1988), and thus it has been the one employed in the results presented. The longitudinal derivative in the first of conditions (7) for the Poisson equation is evaluated staggered starting from a reference point where condition (8) is imposed.

3.2. *Membrane problem*

The membrane equilibrium equations (18) are discretized at every point. The deformations of each segment connecting two points are evaluated by performing longitudinal derivatives on a staggered grid and the membrane stresses (20) over each computational point are obtained averaging the right and left values. Using such a staggered technique each point has a stronger relation firstly with itself and secondly with its neighbours. If centred differentiation is used the membrane stresses depend weakly on the position of the point itself, because derivatives in equation (16) for λ_1 would depend on neighbours only, and lowest wavenumber instabilities can arise.

Boundary conditions (21) are imposed at the left- and right-most points; at the first membrane point on both sides the longitudinal equilibrium equation only is verified and the condition that $R'(\pm L/2) = 0$ is approximated with a third-order formula.

3.3. *Coupled marching*

The time-dependent fluid–membrane problem represents a strongly interacting system whose solution must be obtained by a coupled solution of the fluid and membrane equations (Luo & Pedley 1996) and the alternating solution of the fluid equations and of the membrane equation leads to a rapidly diverging algorithm. This has been

verified in the present case and also in the oversimplified condition of a plane moving boundary with only radial motion, i.e. one degree of freedom (F. Domenichini, private communication).

The coupled algorithm is arranged as follows: once all variables are known at a certain instant, the vorticity at all internal points is advanced in time by the vorticity equation, then the nonlinear system made up of the Poisson equation and the equilibrium equations is solved. During the evaluation of the Poisson equation and the nonlinear set of membrane equations, the vorticity at the wall and the wall pressure are also computed simultaneously because they enter explicitly in the evaluation of the wall stresses to be inserted into the equilibrium equations.

The set of nonlinear equations, can be formally written as $\mathscr{F}_i(Y_j, j = 1, n) = 0$ where the vector Y contains all the unknown functions $Y = [S, R, \psi]$. The system can be formally subdivided into the following parts

$$\left. \begin{aligned} \mathscr{E}(S, R) + \tau(S, R, \psi) &= 0, \\ M(R) \cdot \psi + f(S, R) &= 0; \end{aligned} \right\} \tag{24}$$

the first of (24) represents the set of equilibrium equations where the external loads, τ, depend on the wall geometry and its velocity and on the streamfunction at or near the boundary from formulas (9)–(12). The second of (24) is the linear system corresponding to the discrete version of the Poisson equation, the matrix M depends on the wall geometry, and the term f, once vorticity at the internal points is given, depends on the geometry and on wall velocity. Note that wall velocity is not written explicitly because, as a previous wall configuration is known, it depends only on the new wall configuration.

The nonlinear system (24) is solved by the globally convergent Newton method (Press *et al.* 1992) with small modifications specific to the present problem to improve performance. At each iteration step during the Newton method the solution of a linear system is required whose matrix is given by the Jacobian of equation (24) $\partial \mathscr{F}_i / \partial Y_j$. The linear system is of a sparse type and is solved by the bi-conjugate gradient stabilized method (van der Vorst 1992; Pedrizzetti & Novikov 1994; Pedrizzetti 1996) with a tridiagonal preconditioning to improve convergence speed.

Several difficulties arise in the solution of the nonlinear system: the Newton method at each time step must determine the small corrections (of order of the time step or smaller) to the previous configuration and, within the iterative Newton method, the Jacobian linear system must determine the even smaller corrections. Furthermore, the Jacobian matrix must be evaluated numerically because no explicit dependencies can be easily obtained in the system (24) with the exception of the part of the Jacobian which is equal to the matrix M. All these concurrent difficulties may corrupt the solutions because of comparable tolerances during the steps and limitations of machine precision. A wide investigation has been performed to verify that no numerical disturbances enter into the results: if the Newton method convergence tolerance is assumed as ϵ, the convergence criterion requires $\|\mathscr{F}\| < \epsilon$ or the norm of the correction in one iteration to be less than $10^{-1}\epsilon$; the convergence criterion for the linear system is $10^{-1}\epsilon$. In the following we choose $\epsilon = 10^{-6}$ with double precision computation; however, results are indistinguishable if $\epsilon = 10^{-5}$ is used instead. In addition, as the most critical parts of the nonlinear system are given by the equilibrium equations, the unknown $S(x)$ and $R(x)$ which experience small variations are substituted with their time derivatives $\dot{S}(x)$ and $\dot{R}(x)$ from which the geometry is obtained by time integration.
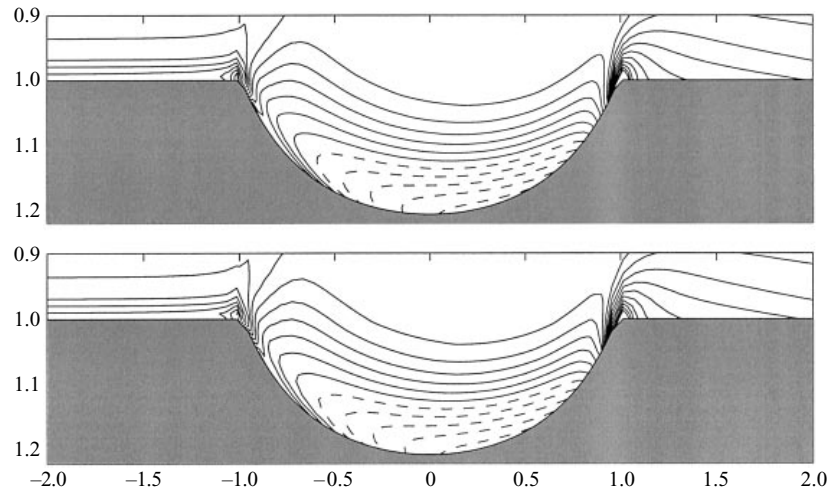
FIGURE 1. Instantaneous vorticity contours during the initial transient for $K = 50$, $C = 10$, $p_{ref} = 10$ obtained with a 192×48 grid (*a*) and a 128×32 grid (*b*); not to scale. Levels from -2.25 to 8, step 0.5; negative levels are dashed.

Initial conditions at $t = 0$ must be chosen such that the system is not too far from its equilibrium solution to avoid either stability problems or a too long transient. In all cases presented below the wall is assumed as initially deformed by a static constant pressure corresponding to its reference value. The fluid motion over the rigid deformed membrane is then evolved until it reaches a steady state (in the unsteady cases the system is left evolving during one time unit). At this point the coupled fluid–membrane evolution is started. This method corresponds to introducing a small but finite perturbation to the system which will then evolve towards its steady or unsteady equilibrium configuration.

3.4. *Numerical parameters and their validation*

The solution of the large nonlinear system (24) represents a substantial time consuming computation. In order to be able to perform an exhaustive analysis the computational grid should be taken as small as possible within the limit of physical significance. After a wide testing of the variation of numerical parameters it has been found that, when the membrane length is $L = 2$, a 128×32 grid in the $\{\eta, \zeta\}$-plane is sufficient to accurately describe the evolution taking stretching parameters $a = 1.6$ and $b = [3, 0.25, 0.5]$. As well as the many trials, a few short runs with grid refinement using 192×48 points and grid coarsening with a 92×24 mesh have also been performed systematically for the physical parameters of §4.1, i.e. $K = 50$, $C = 10$, $p_{ref} = 10$.

The solutions remain stable in all three cases indicating the absence of important unresolved physical features. The analysis of the relative differences in the vorticity fields confirms the appropriateness of the medium resolution grid. In figure 1 the vorticity field during the initial transient is reported as computed with the 192×48 (*a*) and 128×32 grids (*b*). The fields are essentially the same (relative differences below 1%); the largest difference (4%) is found at the wall at the two points corresponding to the rigid–elastic junctions.

The time step is chosen in order to guarantee all the convective and diffusive stability conditions (Fletcher 1988). As an indication a time step of $1/256$ has been used for the 128×32 grid; among the several checks performed in different conditions,
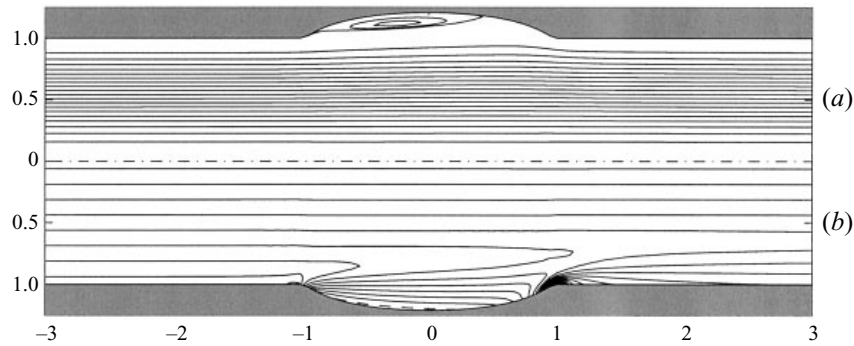
FIGURE 2. Instantaneous streamlines (*a*) and vorticity contours (*b*) in the steady state for $K = 50$, $C = 10$, $p_{ref} = 10$. Streamfunction levels from 0 to 0.5, step 2.5×10^{-2} and from 0.5 to 0.6, step 2.5×10^{-4}; vorticity levels from -0.75 to 10, step 0.5, negative levels are dashed.
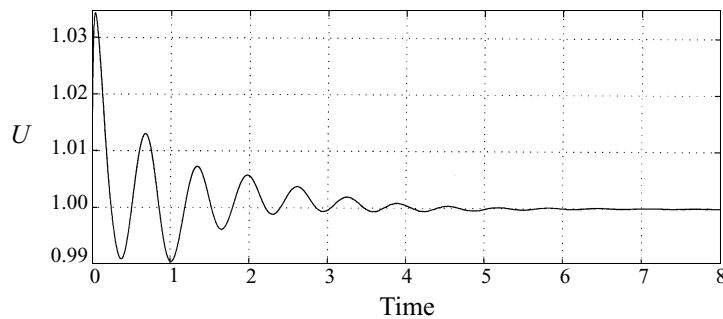

FIGURE 3. Evolution of the upstream mean velocity for $K = 50$, $C = 10$, $p_{ref} = 10$ and steady forcing.

time accuracy has been verified on such a grid employing smaller time steps up to $1/1024$.

On average the numerical computation of the coupled evolution during one time unit requires about 2 CPU hours on a workstation DEC $\alpha 3000/800$ (Specint92 120, Specfp92 184).

4. Results

4.1. *Viscoelasticity*

The onset of steady flow and the dynamics of the transient behaviour are analysed here. Let us first assume the following figures for the various dimensionless parameters: the reference wall pressure is taken as $p_{ref} = 10$ one diameter downstream of the membrane and the flow is forced by a steady discharge, $\varepsilon = 0$, in the downstream rigid duct. As the maximum membrane deformation is approximately given by p_{ref}/K the elasticity parameter is assumed to be $K = 50$ which gives a membrane expanded up to about $R \simeq 1.2$. The wall viscous parameter is assumed, as a starting point, to be $C = 10$ resulting in a damping of fluctuations with timescale smaller than about 0.2.

The system is stable and converges to the steady regime reported in figure 2. The membrane has an almost symmetric shape and the flow presents a weak recirculating region on the upstream part of the enlargement. The velocity averaged in a cross-section of the upstream rigid duct during the transient dynamics is plotted in figure 3.
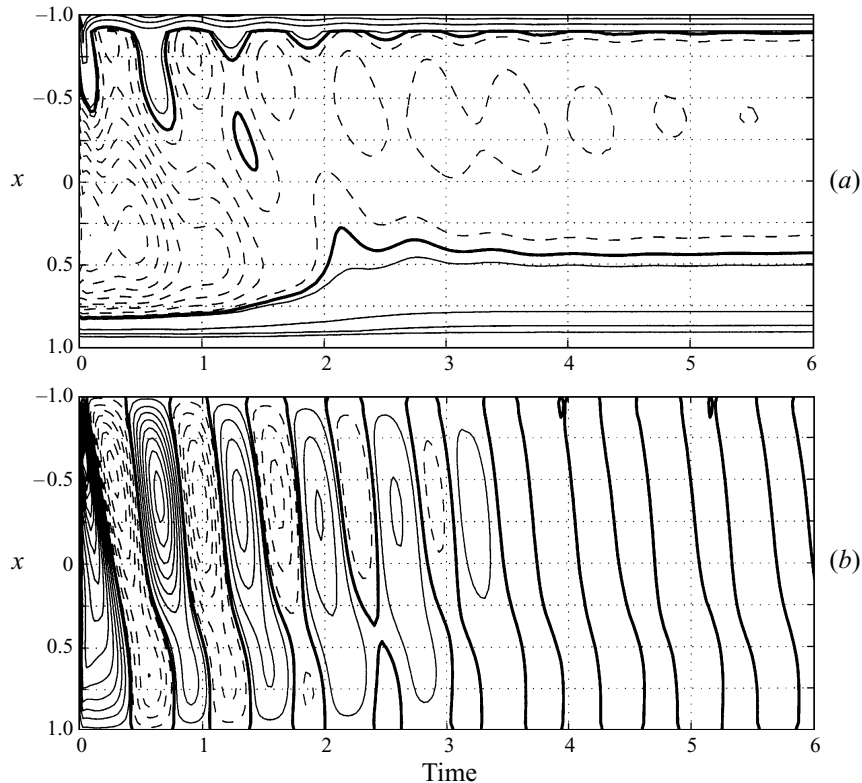
FIGURE 4. Space-time evolution of the wall shear stress (a) and radial wall velocity (b) for $K = 50$, $C = 10$, $p_{ref} = 10$ and steady forcing. Stress levels from -7.5×10^{-3} to -0.5×10^{-3}, step 10^{-3} and from 0.5×10^{-3} to 15.5×10^{-3}, step 5×10^{-3}; velocity levels from -6.5×10^{-3} to 16.5×10^{-3}, step 10^{-3}. The thick lines indicates the zero level, negative levels are dashed.

The transient evolution presents an exponential decay with damped oscillations having constant period. Such an oscillatory behaviour corresponds to membrane waves travelling with positive celerity; the value of the period is evaluated by spectral analysis giving $S_t \simeq 1/0.65$. These waves start upstream and propagate downstream. In fact the flow is forced with a fixed pressure downstream and therefore the maximum oscillation of pressure and consequently of the membrane occurs on the opposite part of the membrane. The space-time development of wave propagation can be observed in figure 4 where the evolution of the wall vorticity (a) and of the radial wall velocity U_r are reported. Tongues of positive vorticity enter the membrane when the membrane velocity is positive, i.e. outwards, because the flow is accelerated and the boundary layer detachment is consequently inhibited. The separated region occupies initially almost the whole membrane and is then rapidly reduced approaching the steady state. The radial velocity plot shows that celerity is everywhere positive with an almost constant value along the membrane length. The longitudinal membrane velocity U_x, which presents the same periodicity, is almost uniform along the membrane and oscillates steadily indicating an approximately uniform longitudinal deformation as assumed in Luo & Pedley (1996).

The viscous behaviour derives either from the fluid or from the membrane by virtue of viscoelastic relation (20). The influence of membrane viscosity is explored by repeating the same calculation with C ranging from 5 to 20; the global result is
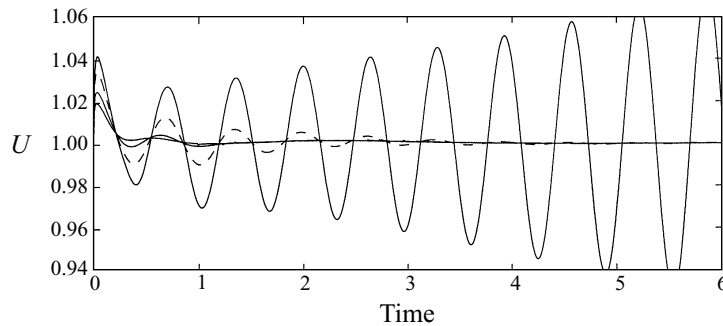
FIGURE 5. Evolution of the upstream mean velocity for $K = 50$, $p_{ref} = 10$, steady forcing, and $C = 7.5, 10, 15, 20$ in the order from the largest to smallest oscillation amplitudes. The dashed line corresponds to $C = 10$.
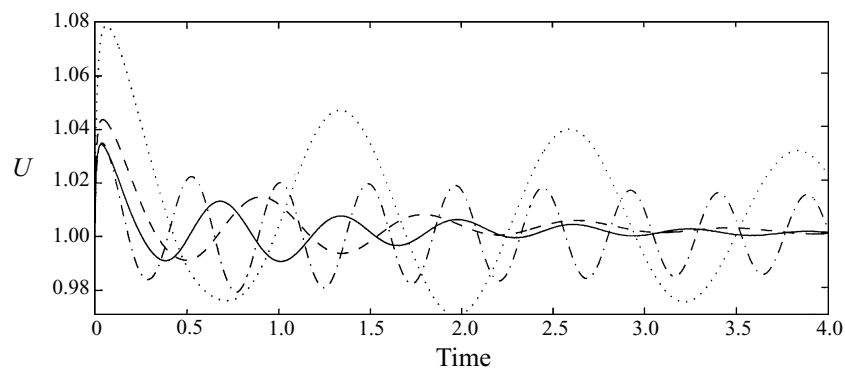

FIGURE 6. Evolution of the upstream mean velocity for steady forcing and different parameters $[K, C, p_{ref}]$. Dash-dot line: [100,10,10]; continuous: [50,10,10]; dashed: [25,8,5]; dotted: [10,4,2].

reported in figure 5. The stability of the fluid–structure interaction depends critically on the value of C. As could be expected for $C > 10$ the viscous phenomena are more relevant and the flow stability is enhanced: for $C = 15$ the system exhibits the same decaying oscillatory behaviour and for $C = 20$ oscillations are almost completely damped because the viscous time scale C/K becomes very close to the natural period. When the value of wall viscosity is reduced to $C = 7.5$ the flow is weakly unstable and the oscillation amplitude presents a slow exponential growth; when $C = 5$, which is not reported in the graph, the oscillation reaches values comparable with unity before $t = 3$. It is worth noting that the period of oscillation is not affected by membrane viscosity and remains the same in all the calculations. We may conclude that the viscous character of the membrane, at least in the present fluid–membrane configuration, cannot be neglected: it plays an essential role in the achievement of steady solutions and in the stability of the system.

An analysis of the influence of the elasticity parameter K is firstly made by taking $K = 100$ and keeping all other values as constant. As could be expected the wall deformation is reduced by about 50% (maximum radius equal to 1.09) and the wave period becomes about 0.48. The evolution of the upstream mean velocity is reported in figure 6 with dash-dot line which must be compared with the previous case plotted with a continuous line. The oscillatory behaviour is less damped with respect to the previous case of a less rigid wall. An explanation may be given by considering that
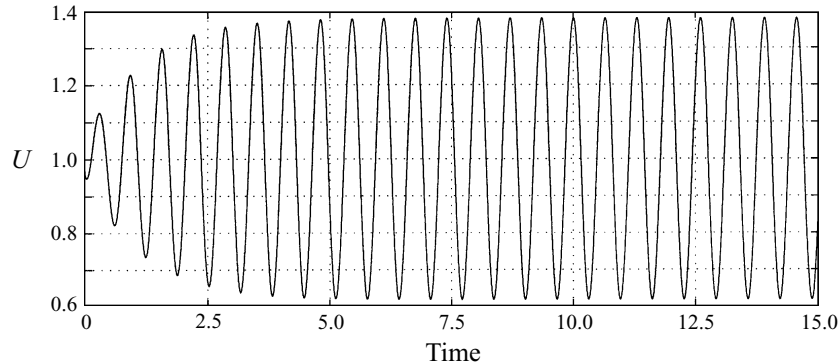
FIGURE 7. Evolution of the upstream mean velocity for $K = 50$, $C = 10$, $p_{ref} = 10$ and unsteady forcing $\varepsilon = 10^{-2}$, $S_t = 0.65^{-1}$.

the time scale of viscous damping is proportional to the value of the ratio C/K which is halved. However, such reasoning is not actually correct. In fact the time scale of oscillation is also reduced proportionally to, assuming valid the linear approximation, about $K^{-1/2}$ (see below) and thus a more correct damping factor can be obtained by the ratio between the two time scales, i.e. $C/K^{1/2}$, which is reduced by a factor of $\sqrt{2}$. Calculations for a more flexible membrane are also reported on the same picture. In order to get results comparable with the first case, when the value of elasticity is decreased the reference pressure is also reduced to keep the ratio p_{ref}/K constant and equal to 0.2. The dashed line corresponds to the result obtained with $K = 25$ and viscosity $C = 8$: comparison with the continuous line shows that the amplitude is initially larger because of the larger membrane flexibility while the damping appears slightly more pronounced as the ratio $C/K^{1/2}$ is increased. The dotted line shows the outcome from a computation with $K = 10$ and $C = 4$. The oscillation is weakly decaying, the ratio $C/K^{1/2}$ being reduced. The period of oscillation takes the values 0.48, 0.65, 0.86, 1.25 with decreasing K from 100 to 10. Its K-dependence, in the first instance, can be approximated by the linear theory (Lighthill 1978), assuming the period to be proportional to the ratio between membrane length and elastic celerity, this gives $S_t \propto K^{1/2}$.

4.2. *Resonance*

The previous subsection has shown that the transient from a non-equilibrium configuration to the steady state develops as waves propagating along the membrane length with a natural frequency. We analyse here the response of the membrane to an unsteady forcing and the occurrence of resonance phenomena.

Let us consider the reference case of §4.1, with parameters vector $[K, C, p_{ref}]$ equal to $[50, 10, 10]$, in which case the natural Strouhal number is $S_t = 0.65^{-1}$. If a pulsatile flow rate is imposed in the downstream duct we should expect a resonance when the Strouhal number is comparable with the natural value. This is shown in figure 7 where the inlet mean velocity is plotted for an outflow given by (1) with $\varepsilon = 10^{-2}$ and $S_t = 0.65^{-1}$. The response of the system reaches a steady oscillation of sinusoidal type $U = 1 + A_\varepsilon \sin(2\pi S_t t + \varphi)$ whose amplitude $A_\varepsilon \simeq 38\varepsilon$. The value of amplification depends on the value of membrane viscosity C; the fact that the output is essentially a sinusoidal signal with negligible energy in other frequencies suggests that despite its complexity the system has a quasi-linear response. The instantaneous
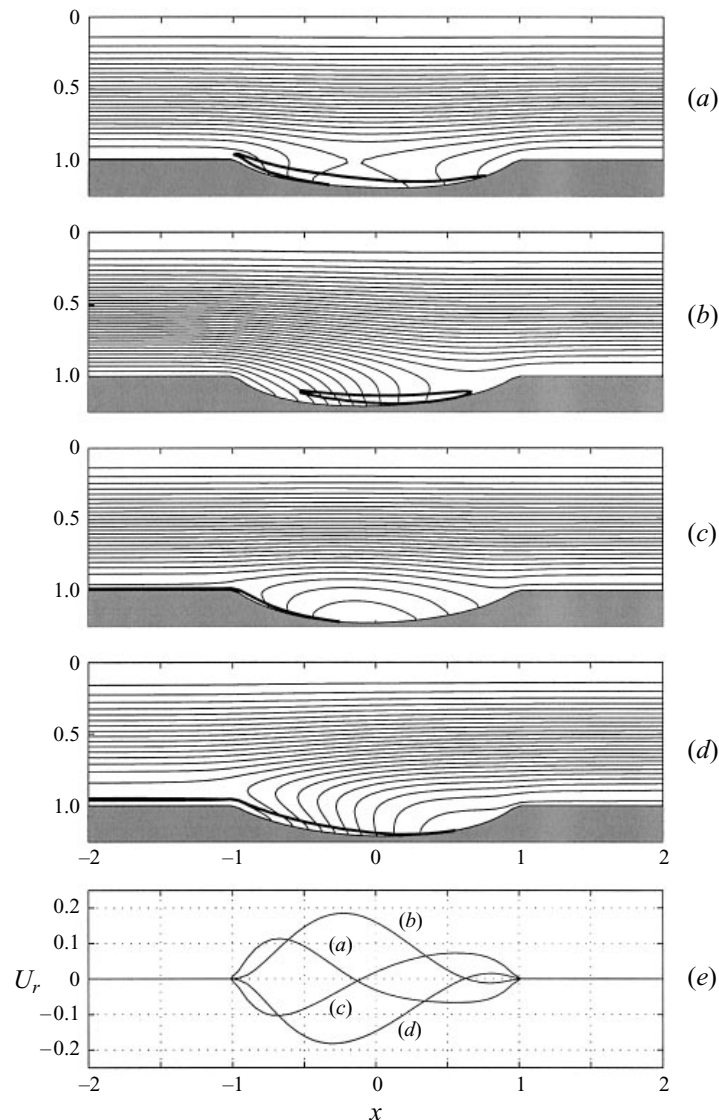
FIGURE 8. Oscillatory flow for $K = 50$, $C = 10$, $p_{ref} = 10$ and unsteady forcing $\varepsilon = 10^{-2}$, $S_t = 0.65^{-1}$. Instantaneous streamlines at (a) 0/4, (b) 1/4, (c) 2/4, (d) 3/4 of the period of upstream flow oscillation, streamfunction levels from 0 to 0.7, step 0.02, the thick lines corresponds to the zero vorticity contour. (e) Corresponding membrane radial velocity.

flow field at four instants during the steady oscillatory regime is given in figure 8. The streamlines and the zero vorticity contour (thick line) are reported during one oscillation at four equispaced instants corresponding to an accelerating upstream flow, maximum velocity, decelerating flow, minimum velocity; the corresponding radial membrane velocity is reported on the bottom of the same figure. The behaviour of the streamlines which terminate on the moving membrane is of interest. In figure 8(a) the instantaneous value of the accelerating upstream flow is comparable with the downstream one and thus some streamlines enter the membrane from upstream and exit to downstream; this can also be verified from the corresponding radial
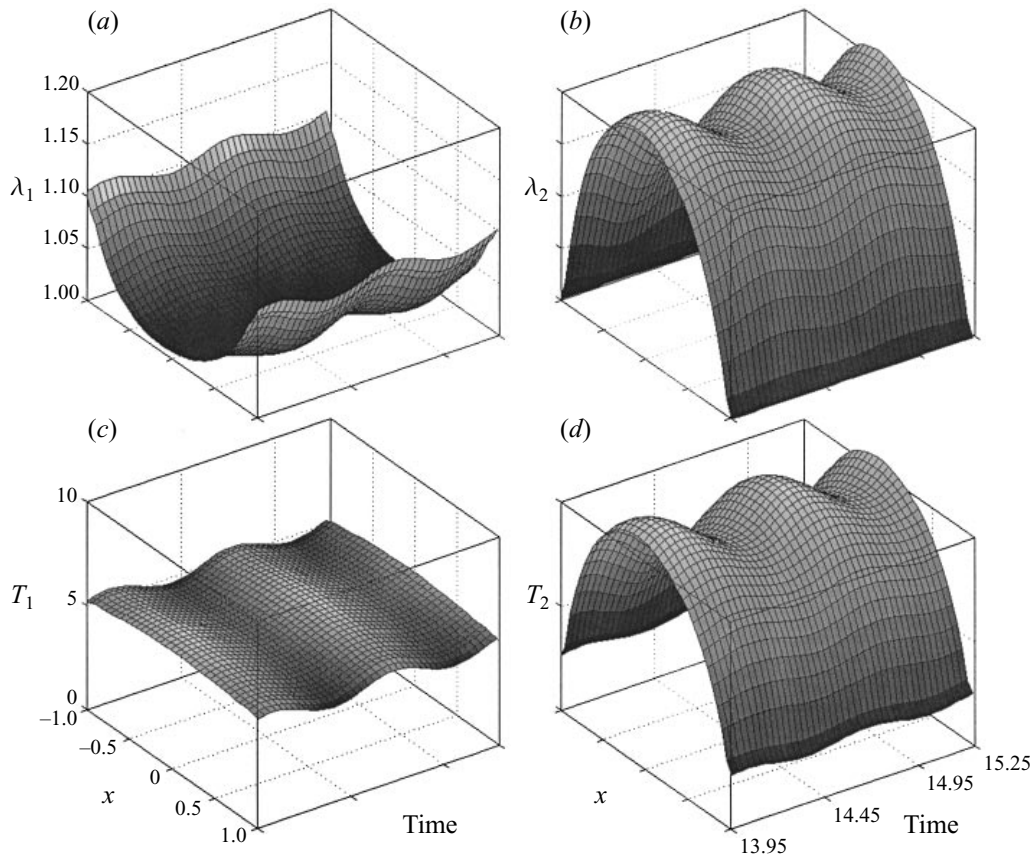
FIGURE 9. Space-time evolution of deformation eigenvalues (*a,b*) and membrane stresses (*c,d*) for $K = 50$, $C = 10$, $p_{ref} = 10$ and unsteady forcing $\varepsilon = 10^{-2}$, $S_t = 0.65^{-1}$, during two oscillations.

membrane velocity. In figure 8(*b*) the membrane is enlarging (positive U_r) and sucks in the flow coming from upstream, in figure 8(*c*) the upstream and downstream flow are comparable and, as a complementary configuration with respect to 8(*a*), the up- and downstream membrane portions compensate each other creating closed streamlines. Finally, when the upstream flow is slow the membrane shrinks.

The space-time evolution of the longitudinal and circumferential eigenvalues λ_1 and λ_2 and static membrane stresses T_1 and T_2 are reported in figure 9; note that the second eigenvalue is exactly the membrane geometry $R(t, x)$. The membrane is substantially stretched longitudinally near the junctions while the radial displacement is maximum in the middle and dominates the overall deformation. Previous works (Luo & Pedley 1996) concerning two-dimensional flow, and thus a one-dimensional membrane, have assumed that the longitudinal stress was uniform along the membrane and constant in time. In this case longitudinal deformation is not uniform nor constant in time; however, there is not a direct scalar proportionality between stress and strain because the two-dimensional shape of the membrane involves the interaction between longitudinal and circular stresses (20). After this combination the longitudinal stress is indeed about uniform (its average value ranges from 5.2 to 5.5 along x) even though it presents a non-negligible oscillation in time (average ranges from 5 to 5.7). The transversal membrane stress is dominated by circular strain everywhere apart
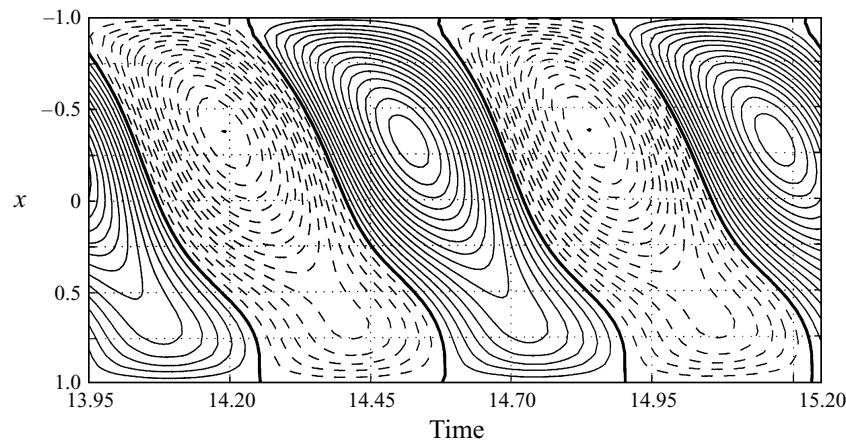
FIGURE 10. Space-time evolution of membrane radial velocity for $K = 50$, $C = 10$, $p_{ref} = 10$ and unsteady forcing $\varepsilon = 10^{-2}$, $S_t = 0.65^{-1}$, during two oscillations. Velocity levels from -0.2 to 0.2, step 0.0125. The thick lines indicates the zero level, negative levels are dashed.

from the membrane ends where longitudinal elongation is relevant. The space-time evolution of the membrane radial velocity is reported in figure 10 by a contour plot. It clearly shows the presence of a propagation phenomenon with positive celerity. The maximum disturbance occurs upstream, i.e. farther from the point where pressure is fixed, and propagates downstream. This space-time propagation phenomenon is shared by all quantities, including the longitudinal strain, with the exception of the axial velocity and the longitudinal stress.

Note at this point that the maximum difference between the normal stress (10) and pressure is less than 0.1% during the whole oscillation while the maximum difference between the tangential stress (11) and the term $R_e^{-1}\omega$ is less than 3%.

In order to verify the presence of a real resonance phenomenon, several simulations have been performed with the same parameters and varying the Strouhal number of the imposed oscillation from 0.68 to 2. In all cases the system reaches a steady oscillatory regime with the amplitude of upstream flow oscillation larger than the downstream forcing value ε. The spectral analysis of the signal indicates that oscillations are essentially of sinusoidal type with a non-zero but small energy in frequencies that are multiples of the forcing value. The only difference has been observed when the Strouhal number is exactly one half of the natural one; in this case some energy also accumulates in correspondence with the natural frequency and the response is a combination of two sinusoidal signals with amplitude ratio about five. These results indicate that the system behaves approximately like a linear one and some simple nonlinearity, i.e. excitation of multiple frequencies, can be observed only when enhanced by resonance. The dependence of the amplitude of the response with respect to the Strouhal numbers is sketched in figure 11: the computed values are reported with circles and the dotted line indicates an arbitrarily drawn approximation. The picture, where the amplitude depends on the value of C, is analogous to the resonance plot for a linear system.

Several simulations have been performed with different values of the elasticity and reference pressure for the results presented in figure 6. In all cases the same behaviour has been observed.
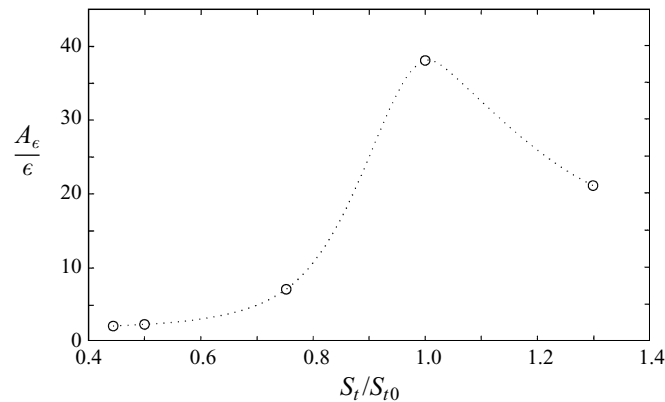
FIGURE 11. Ratio of up- and downstream oscillation amplitudes versus ratio of the forcing and natural Strouhal numbers for $K = 50$, $C = 10$, $p_{ref} = 10$. Circles are results from simulations; the dotted line is an arbitrary approximation.

4.3. *Symmetry breaking on up- and downstream conditions*

The results reported so far assume that the discharge is imposed on the rigid duct downstream of the membrane so that the pipe works by suction. Unless we have an exact reference physical phenomenon to reproduce, this choice is arbitrary. In this subsection we try to draw some conclusion from the previous results for the dual case when the discharge is imposed in the upstream duct, and we complete the discussion by commenting on some additional results.

Let us consider the steady oscillatory regimes of §4.2. In all these a small oscillation in the downstream flow provokes a larger oscillation at the inlet. By symmetry considerations we can also conclude that the same fluid–membrane system with an imposed oscillation in the upstream flow leads to a downstream flow where oscillations are damped. That is: the resonating system discussed above can be seen as an oscillation-damper from upstream to downstream with the same type of characteristic curve as the one sketched in figure 11. The maximum efficiency in damping occurs when oscillations have a period close to the natural one so that the membrane is able to better absorb the incoming fluctuations.

This symmetry argument does not account for stability. It may be invalidated only if a solution which is stable in one case happens to be unstable in the inverse system. In addition, these consideration are valid for steady flow and for stable oscillatory regimes. We cannot draw any conclusion in such terms about the transient phase of the flow, and neither can we say anything about the behaviour of the system for parameter values, namely low membrane viscosity, which have exhibited an unstable behaviour.

Numerical simulations have been performed for the sets of parameters used in §4.2 above and imposing the flow rate upstream of the membrane. It has been verified that exactly the same stable regime of figures 7–10 could be found, indicating the validity of the symmetry argument expressed above.

Let us now consider a perfectly elastic membrane, $C = 0$. This has been seen above to develops unstable travelling waves when the system is forced with a downstream flow rate. In the symmetric case, when a unit discharge is imposed upstream of the membrane, the calculations show that the flow is stable and converges towards a steady configuration even in the absence of membrane viscosity. The transient
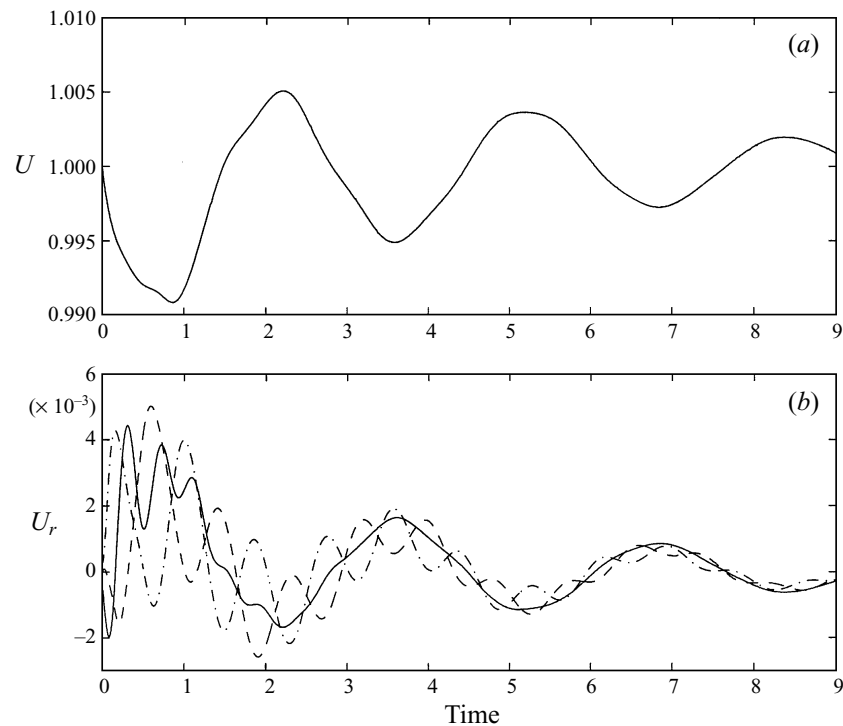
FIGURE 12. Evolution of the downstream mean velocity (*a*), and (*b*) radial membrane velocity at $x = -L/4$ (dashed line), $x = 0$ (continuous), $x = L/4$ (dash-dot), for $K = 50$, $C = 0$, $p_{ref} = 10$ and steady forcing.

evolution of the downstream discharge is shown in figure 12(*a*) for $K = 50$, $p_{ref} = 10$. The system presents a natural oscillation with a period of about 3.25 time units. Such an oscillation is not associated with a propagation phenomenon and corresponds to a synchronous movement of the wall with wavelength equal to twice the membrane length, i.e. the first natural mode. On top of this another static fluctuation with half a wavelength is present on the membrane corresponding to the second natural mode, with an apparently unrelated period equal to 0.845 time units. In the second mode when half the membrane expands the other half contracts giving null integral contribution to the flow rate. This behaviour can be seen in figure 12(*b*) which reports the evolution of the radial wall velocity, U_r, in the middle of the membrane (continuous line) and at one and three quarters of the membrane length. The central point exhibits only the long wavelength mode, while up- and downstream of this the wall moves, in alternation, also for the second mode. No wave propagation can be seen; we can conjecture that the previously observed instability corresponds to a complete damping of such a phenomenon in the inverse system.

The perfectly elastic membrane remains stable even when a pulsatile upstream discharge is imposed. This has been checked for the natural frequencies of the travelling wave, $S_t = 0.65^{-1}$, and of the second steady mode, $S_t = 0.845^{-1}$. The discharge oscillations are reduced in amplitude at the downstream end, the phenomena involved are similar for both cases and no travelling wave appears. The evolution of the downstream mean velocity, and the space-time pattern of the radial membrane velocity are
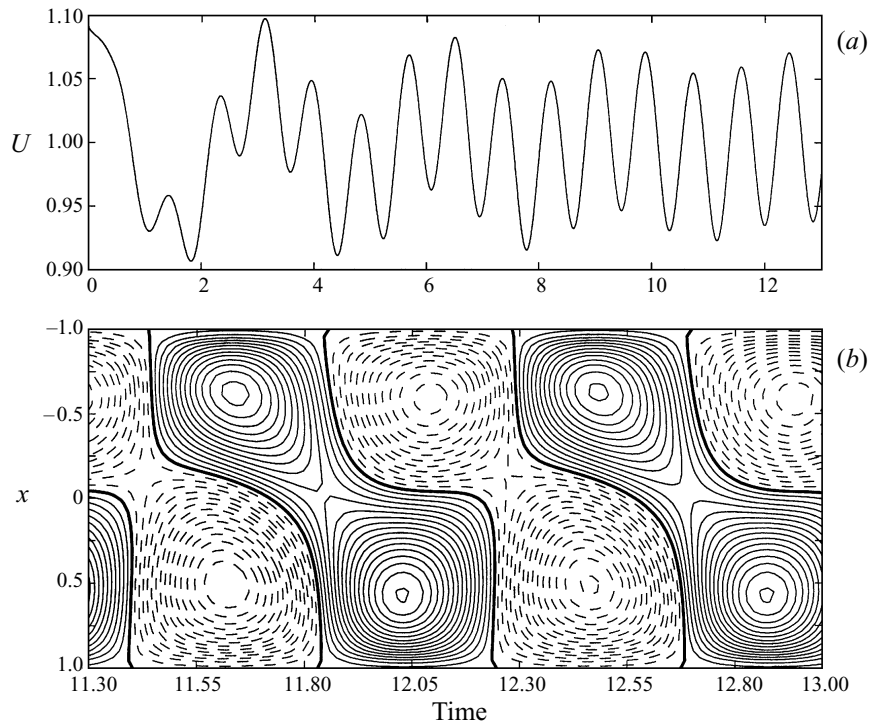
FIGURE 13. Evolution of the downstream mean velocity (*a*), and (*b*) space-time evolution of membrane radial velocity during two oscillations for $K = 50$, $C = 0$, $p_{ref} = 10$ and unsteady forcing $\varepsilon = 10^{-1}$, $S_t = 0.845^{-1}$. Velocity levels from -0.2 to 0.2, step 0.0125. The thick lines indicates the zero level, negative levels are dashed.
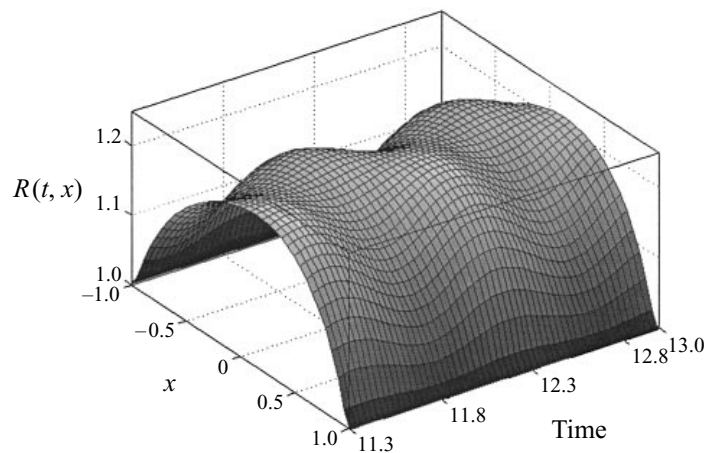

FIGURE 14. Space-time evolution of membrane wall for $K = 50$, $C = 0$, $p_{ref} = 10$ and unsteady forcing $\varepsilon = 10^{-1}$, $S_t = 0.845^{-1}$, during two oscillations.

reported in figure 13 for the latter case for $\varepsilon = 10^{-1}$. The resulting fluctuations are non-propagating with wavelength equal to the membrane length and the contribution to the flow rate is given by their slight non-symmetry. The membrane deformation is shown in figure 14 where the alternating distortion is observable. It is relevant to point out that the same computation with $C = 10$ leads to the travelling wave regime only.
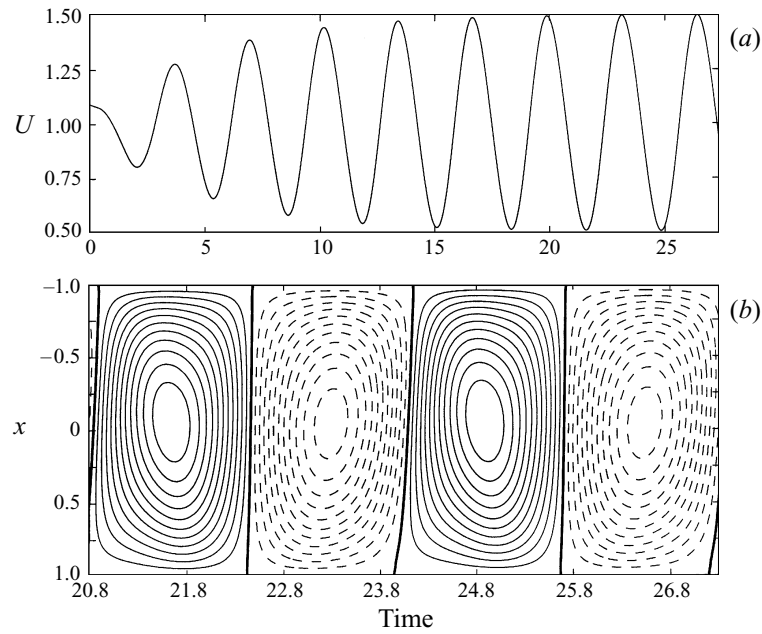
FIGURE 15. Evolution of the downstream mean velocity (*a*), and (*b*) space-time evolution of membrane radial velocity during two oscillations for $K = 50$, $C = 0$, $p_{ref} = 10$ and unsteady forcing $\varepsilon = 10^{-1}$, $S_t = 3.25^{-1}$. Velocity levels from -0.2 to 0.2, step 0.0125. The thick lines indicates the zero level, negative levels are dashed.
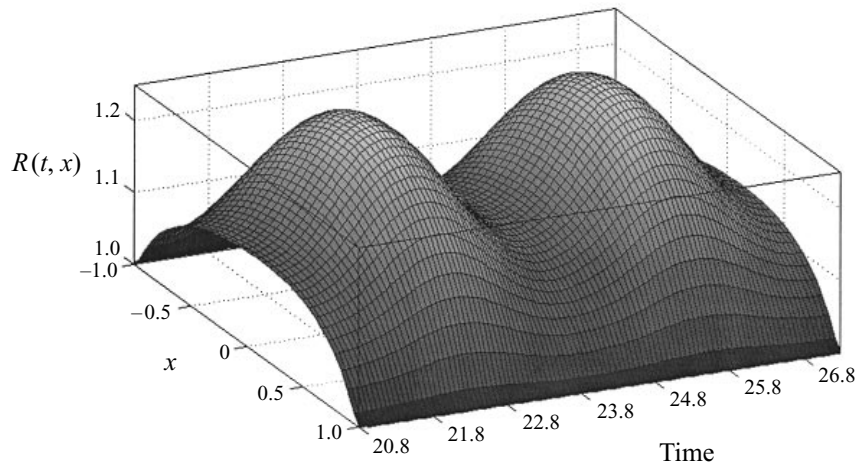

FIGURE 16. Space-time evolution of membrane wall for $K = 50$, $C = 0$, $p_{ref} = 10$ and unsteady forcing $\varepsilon = 10^{-1}$, $S_t = 3.25^{-1}$, during two oscillations.

A resonance can also be expected if the upstream pulsation has a frequency comparable with the fundamental mode, $S_t = 3.25^{-1}$. The downstream mean velocity and the space-time pattern of the radial membrane velocity are reported in figure 15, for $\varepsilon = 10^{-1}$. The discharge is amplified about 5 times, and the membrane presents a synchronous oscillation at all points as can also be noticed by the time evolution of the wall profile depicted in figure 16. As in the case of propagating waves the longitudinal

stress is approximately uniform along the membrane even if the longitudinal strain is not.

Other results have been obtained by putting the elasticity parameter and reference pressure to the values of figure 6. The same phenomena have been observed for such values and the natural period of oscillation varies approximately proportionally to $K^{-1/2}$ as indicated by the linear theory. To complete the analysis it has been also verified that if a fixed pressure is imposed upstream then, with given downstream discharge, the phenomena discussed so far still hold, but when the discharge is imposed upstream the oscillation propagates with negative celerity.

5. Conclusions

The unsteady flow in a circular tube with an elastic insertion has been solved numerically. The theory of elastic membranes under finite deformation has been adapted to permit its link to the fluid equations. A numerical method for the simultaneous solution of the unsteady fluid–membrane problem has been presented.

A positive transmural pressure has been imposed downstream of the membrane, thus the elastic wall is expanded outwards.

When a steady fluid discharge is imposed on the downstream rigid duct the fluid–wall interaction develops travelling waves along the membrane whose period depends on membrane elasticity. The waves develop near the upstream end where pressure fluctuations are larger and propagate with positive celerity. The interaction is stable only if the value of membrane viscosity is larger than a critical limit. In these cases a resonance of the fluid–wall interaction occurs if a pulsatile flow–rate with frequency close to the natural one is imposed. Each quantity reaches a steady oscillatory regime due to the continuous propagation of membrane waves. Observation of the upstream flow indicates that the system as a whole, forced by a sucked flow, presents a behaviour close to linear.

Travelling waves in a tube undergoing suction are stable only if wall viscosity is large enough. This reflects in the behaviour of the system with discharge value imposed upstream. For the same stable parameters when a pulsatile flow is imposed at the inlet, after a different transient, the system reaches the same oscillatory regime. Qualitatively different phenomena occur for a membrane whose viscosity is low enough that travelling waves were unstable. The presence of an upstream imposed flow and a downstream fixed pressure results in a bigger degree of constraint on the system which is stable even if the membrane is perfectly elastic. In this case the system presents two natural frequencies associated with static oscillations where waves are absolutely damped. These correspond to a synchronous membrane movement and to a secondary oscillatory mode with wavelength equal to the membrane length. A forcing with the corresponding frequencies results in static fluid–membrane resonance phenomena which disappear if the value of wall viscosity is increased leaving wave propagation only.

The stationary oscillations observed here may be related to the so-called divergence boundary-layer instability (Lucey & Carpenter 1992 and references therein) predicted in a two-dimensional flow over compliant wall which can be stable if the finite-length movable wall is perfectly elastic or slightly viscoelastic. Its development in a circular tube has not been analysed previously and comparisons are unattainable. Remarkable differences with the two-dimensional results are obvious but we cannot argue on the basis of these simple observations whether the phenomenon is the same. In particular the correspondence of oscillation wavelengths and membrane length

is not a prerequisite; furthermore, the increase in wall damping does not lead to instability but to the onset of travelling waves.

In all cases no self-excited oscillation, like those observed in a two-dimensional channel with a finite constant-tension membrane on one side (Luo & Pedley 1996), were found. In that case the channel is close to collapse, membrane stress is extremely low, and the fluid has a separation point. The interaction between a loose wall and separated vorticity, that is essentially absent in the present work, plays a relevant role in self-excitation. Similarly, the development of chaotic fluctuations argued in Luo & Pedley (1996 and references therein) and observed in a one-dimensional model of a collapsible tube (Jensen 1992) have not been found here. In the present case the smaller membrane length and the axial symmetry result in a higher degree of constraint of the system. However the presence of different excitable frequencies may result in their nonlinear interaction in some special region of the high-dimensional space of parameters.

The results, even though within a limited range of parameters, give some insight into the unsteady phenomena occurring in the fluid–structure interaction. The criticality of some of them and of actual boundary conditions show that very precise indications about the physical system to be modelled are required to produce reliable results. The present observations can also provide a basis for future development of fluid–membrane interaction, and for the more complex phenomenon of flow in a contracted area. In that case the axisymmetric membrane geometry is unstable, and work is currently in progress to model the full two-dimensional membrane surface and its non-circular deformation occurring when transmural pressure assumes instantaneous negative values.

REFERENCES

ARAKAWA, A. 1966 Computational design for long term numerical integration of the equation of fluid motion: Two dimensional incompressible flow. Part I. *J. Comput. Phys.* **1**, 119–143.

BATCHELOR, G. K. 1967 *An Introduction to Fluid Dynamics.* Cambridge University Press.

CANCELLI, C. & PEDLEY, T. J. 1985 A separated-flow model for collapsible-tube oscillations. *J. Fluid Mech.* **157**, 375–404.

CARPENTER, P. W. & MORRIS, P. J. 1990 The effect of anisotropic wall compliance on boundary-layer stability and transition. *J. Fluid Mech.* **218**, 171–223.

DAVIES, C. & CARPENTER, P. W. 1997 Numerical simulation of the evolution of Tollmien-Schlichting waves over finite compliant panels. *J. Fluid Mech.* **335**, 361–392.

EISEMAN, P. R. 1985 Grid generation for fluid mechanics computation. *Ann. Rev. Fluid Mech.* **17**, 487–522.

FLETCHER, C. A. 1988 *Computational Techniques for Fluid Dynamics I.* Springer.

FRIED, I. 1982 Finite element computation of large rubber membrane deformation. *Intl J. Numer. Meth. Engng* **18**, 653–660.

GREEN, A. E. & ADKINS, J. E. 1960 *Large Elastic Deformations.* Clarendon.

HSU, F. P. K., SCHWAB, C., RIGAMONTI, D. & HUMPHREY, J. D. 1994 Identification of response functions from axisymmetric membrane inflation tests: implication for biomechanics. *Intl J. Solids Struct.* **31**, 3375–3386.

HUMPHREY, J. D., STRUMPF, R. K. & YIN, F. C. P. 1992 A constitutive theory for biomembranes: application to epicardial mechanics. *J. Biomech. Engng* **114**, 461–466.

JENSEN, O. E. 1992 Chaotic oscillations in a simple collapsible tube model. *J. Biomech. Engng* **114**, 55–59.

JENSEN, O. E. & PEDLEY, T. J. 1989 The existence of steady flow in a collapsed tube. *J. Fluid Mech.* **206**, 339–374.

KUMARAN, V. 1996 Stability of inviscid flow in a flexible tube. *J. Fluid Mech.* **320**, 1–17.

KYRIACOU, S. K. & HUMPHREY, J. D. 1996 Influence of size, shape and properties on the mechanics of axisymmetric saccular aneurysms. *J. Biomech.* **29**, 1015–1022.

LIGHTHILL, J. 1978 *Waves in Fluids.* Cambridge University Press.

LUCEY, A. D. & CARPENTER, P. W. 1992 A numerical simulation of the interaction of a compliant wall and inviscid flow. *J. Fluid Mech.* **234**, 121–146.

LUO, X. Y. & PEDLEY, T. J. 1995 A numerical simulation of steady flow in a 2-D collapsible channel. *J. Fluids Struct.* **9**, 149–174.

LUO, X. Y. & PEDLEY, T. J. 1996 A numerical simulation of unsteady flow in a two-dimensional collapsible channel. *J. Fluid Mech.* **314**, 191–225.

PANTON, R. 1996 *Incompressible Flow.* John Wiley & Sons.

PEDLEY, T. J. 1980 *The Fluid Mechanics of Large Blood Vessels.* Cambridge University Press.

PEDRIZZETTI, G. 1996 Unsteady tube flow over an expansion. *J. Fluid Mech.* **310**, 89–111.

PEDRIZZETTI, G. & NOVIKOV, E. A. 1994 On Markov modelling of turbulence. *J. Fluid Mech.* **280**, 69–93.

PIPKIN, A. C. 1968 Integration of an equation in membrane theory. *Z. Angew Math. Phys.* **19**, 818–819.

PRESS, W. H., TEUKOLSKY, S. A., VETTERLING, W. T. & FLANNERY, B. P. 1992 *Numerical Recipes,* 2nd edn. Cambridge University Press.

REYN, J. W. 1987 Multiple solutions and flow limitation for steady flow through a collapsible tube held open at the ends. *J. Fluid Mech.* **174**, 467–493.

SECOMB, T. W. 1978 Flow in a channel with pulsating walls. *J. Fluid Mech.* **88**, 273–288.

SKALAK, R., TOZEREN, A., ZARDA, A. P. & CHIEN, S. 1973 Strain energy function of red blood cell membranes. *Biophys. J.* **13**, 245–264.

TIELKING, J. T. & FENG, W. W. 1974 The application of the minimum potential energy principle to nonlinear axisymmetric membrane problems. *Trans. ASME*: *J. Appl. Mech.* **June**, 491–496.

VORST, H. A. VAN DER 1992 BiCGSTAB - A fast and smoothly converging variant of Bi-CG for the solution of nonsymmetric linear systems. *SIAM J. Sci. Statist. Comput.* **13**, 631–644.